HAL
open science

Quantum study of the bending relaxation of H2O by collision with H

Lisán David Cabrera-González, Otoniel Denis-Alpizar, Dayán Páez-Hernández, Thierry Stoecklin

To cite this version:

Lisán David Cabrera-González, Otoniel Denis-Alpizar, Dayán Páez-Hernández, Thierry Stoecklin. Quantum study of the bending relaxation of H2O by collision with H. Monthly Notices of the Royal Astronomical Society, 2022, 514 (3), pp.4426-4432. 10.1093/mnras/stac1643 . hal-03855140

HAL Id: hal-03855140

https://hal.science/hal-03855140v1

Submitted on 24 Nov 2022

HAL is a multi-disciplinary open access archive for the deposit and dissemination of scientific research documents, whether they are published or not. The documents may come from teaching and research institutions in France or abroad, or from public or private research centers.

L'archive ouverte pluridisciplinaire **HAL**, est destinée au dépôt et à la diffusion de documents scientifiques de niveau recherche, publiés ou non, émanant des établissements d'enseignement et de recherche français ou étrangers, des laboratoires publics ou privés.

Monthly Notices of the ROYAL ASTRONOMICAL SOCIETY

MNRAS **514,** 4426–4432 (2022) https://doi.org/10.1093/mnras/stac1643

Quantum study of the bending relaxation of H_2O by collision with H

Lisán David Cabrera-González,[1] Otoniel Denis-Alpizar,[2] Dayán Páez-Hernández[1] and Thierry Stoecklin[3]★

[1]*Doctorado en Fisicoquímica Molecular, Facultad de Ciencias Exactas, Universidad Andres Bello, República 275, Santiago, Chile*
[2]*Instituto de Ciencias Químicas Aplicadas, Facultad de Ingeniería, Universidad Autónoma de Chile, Av. Pedro de Valdivia 425, Providencia, Santiago, Chile*
[3]*Institut des Sciences Moléculaires, Université de Bordeaux, CNRS UMR 5255, 33405 Talence Cedex, France*

Accepted 2022 June 9. Received 2022 June 9; in original form 2022 March 23

ABSTRACT

Vibrationally excited levels of the H_2O molecule are currently detected in various environments of the interstellar medium (ISM), and collisional data for H_2O, including vibration with the main colliders of the ISM, are needed. The present study focuses on the bending relaxation of H_2O by collision with H when taking bending–rotation coupling explicitly into account with the rigid-bender close-coupling (RB-CC) method. With this aim, a new four-dimensional potential energy surface including the H_2O bending mode is developed from a large grid of *ab initio* energies computed using a high level of theory. For purely rotational transitions, our RB-CC rates show very good agreement with rigid-rotor calculations performed using our new potential energy surface (PES) and with those available in the literature. Calculations for pure rotational transitions inside the excited bending level $\nu_2 = 1$ of H_2O are performed and compared with their equivalents inside $\nu_2 = 0$. Vibrational quenching of H_2O is also calculated and found to be much more efficient through collision with H rather than with He.

Key words: astrochemistry – molecular data – molecular processes – scattering.

1 INTRODUCTION

H_2O is the third most abundant interstellar molecule. It is detected in astrophysical environments as diverse as star-forming regions, evolved stars, or extragalactic sources, where water masers inside the fundamental vibrational level of H_2O have been observed for many years (see table 6 of Gray et al. 2016). Inside the first excited bending state of H_2O, two pure rotational lines showing weak emission have already been detected by Menten & Melnick (1989) and the $1_{10} \rightarrow 1_{01}$ line was the first strong maser transition of this type to be discovered in 1995 (Menten & Young 1995). Since then, several other very high energy transitions involving excited bending levels of water have been discovered (Hunter et al. 2007; Hirota, Kim & Honma 2016; Baudry et al. 2018), mostly in the extended atmosphere and envelope of evolved O-rich stars of our Galaxy. These transitions are predominantly collisionally pumped (Nesterenok 2015). Also, collisional excitation rates for transitions between the H_2O ground state and vibrationally excited states and for collisions within the excited states are needed to model vibrational excitation of H_2O in circumstellar envelopes. Many rigid-rotor calculations are available for inelastic collisions of water with He, H_2, e^-, or H, and Daniel et al. (2014) found that the rates for He, H_2, and H are very different and cannot be deduced from each other in a simple way.

In several recent theoretical studies, vibrationally inelastic collisions of H_2O with H_2 (Stoecklin et al. 2019), He (Stoecklin et al. 2021), and e^- (Ayouz et al. 2021) were also considered for the first time. In the present work, we complement these data by studying the bending relaxation of H_2O by collision with H atoms. This collision is reactive: $H + H_2O \rightarrow H_2 + OH$, and was the subject of many theoretical studies (Jiang, Xie & Guo 2011; Fu & Zhang 2013; McCarver & Hinde 2021). It is, however, endothermic by 0.64 eV and its activation barrier was found to be 0.84 eV. Also, this system can safely be considered to be inelastic for the lower excited bending levels of H_2O and for collision energies below 5000 cm^{-1} (Van Dishoeck, Herbst & Neufeld 2013).

The only set of inelastic rate coefficients available for this system in the BASECOL database (Dubernet et al. 2013) was calculated by Daniel et al. (2014) and concerns only pure rotational transitions inside the fundamental vibrational level. In the present work, we calculate a new four-dimensional (4D) potential energy surface (PES) including bending and use the rigid-bender close-coupling (RB-CC) method to study water bending relaxation resulting from its collisions with H atoms, along the lines of our previous studies dedicated to the collisions of H_2O with H_2 (Stoecklin et al. 2019) and He (Stoecklin et al. 2021).

This work is organized as follows. The calculations and fitting of the 4D PES, as well as the main steps of the RB-CC calculations, are presented in Section 2. In Section 3, the results for the PES and dynamics are discussed, while in Section 4 a few concluding remarks are made.

2 METHODS

2.1 Potential energy surface

Several good quality non-reactive PESs for the $H_2O + H$ complex are available and could, in principle, be used. However, they were all calculated for a rigid-rotor configuration of H_2O. This is the case

★ E-mail: thierry.stoecklin@u-bordeaux.fr

© 2022 The Author(s)
Published by Oxford University Press on behalf of Royal Astronomical Society

Downloaded from https://academic.oup.com/mnras/article/514/3/4426/6622022 by Universite de Bordeaux user on 01 July 2022

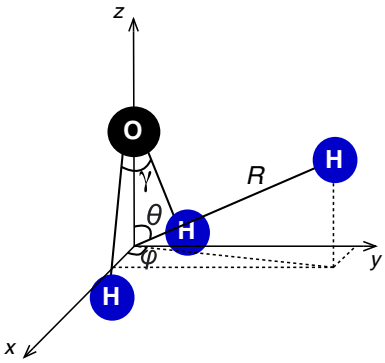

Figure 1. Coordinates for collisions of H_2O with H. The frame origin is the centre of mass of H_2O, which is in the XoZ plane.

for the very recent PES of McCarver & Hinde (2021) and the PES used by (Daniel et al. 2014) to perform dynamics calculations, which were originally developed by Dagdigian & Alexander (2013). Here, a new 4D PES $V(\gamma, R, \theta, \phi)$ including bending motion is required to study collisional bending relaxation, which is presented below.

The H_2O molecule is situated in the XoZ plane of the coordinate system represented in Fig. 1. The H_2O centre of mass is the origin of the frame and the oxygen atom is on the positive side of the z-axis, while the bending angle γ is bisected by the z-axis. On the same figure are also represented the intermolecular vector $\boldsymbol{R}$connecting the H_2O centre of mass to the H atom, the modulus of which is denoted R, θ the angle between the z axis and the intermolecular vector $\boldsymbol{R}$, and φ the azimuthal angle. The OH bond distance was fixed at 0.957 Å (Valiron et al. 2008).

The *ab initio* energies were computed at the UCCSD(T)-F12a level of theory using the aug-cc-pVTZ basis set (Dunning 1989). All calculations were performed with the MOLPRO package (Werner et al. 2012), and the basis-set superposition error was corrected with the counterpoise procedure (Boys & Bernardi 1970). In total, 15 428 *ab initio* energies were computed. The grid included seven values of bending angle γ ranging from 70° to 140°, 29 values of R between 1.3 and 10 Å, 19 values of θ in the (0, 180)° interval, and four values of φ in steps of 30° in the (0, 90)° interval.

$$V(\gamma, R, \theta, \phi) = \sum_{m=0}^{6} \sum_{l=m}^{18} V_{lm}(\gamma, R) P_l^m(\cos\theta)\cos(m\varphi). \quad (1)$$

The analytical form (1) of the intermolecular potential expanded in the usual Green basis set is then obtained by fitting this grid of points using the reproducing-kernel Hilbert-space method of Ho & Rabitz (1996), following the procedure detailed in our previous work dedicated to the H–H_2O system (Stoecklin et al. 2021). The short- and long-range parts of the PES are fitted independently and then assembled using a switching function, while only even values of m are used in (1), as a result of the C_{2v} symmetry of the H_2O molecule.

In order to check the quality of the fitted long-range part, we compared it with the experimental value of the usual following analytical form (Hou et al. 2016):

$$U_{\rm lr} = \frac{C_6(\theta, \varphi)}{R^6}. \quad (2)$$

30 values of R in the interval [5.5,14] Å were used to least-squares fit the isotropic contribution V_{00} of our PES term. This leads to a PES value of $C_6^{\rm PES} = 18.98$ au, which includes both the induction and dispersion contributions. The experimental dispersion value is obtained from known values (Stone 2016) for H_2O–H_2O and H–H interactions, using

$$C_6^{\rm Dis}({\rm H_2O–H}) = \frac{2\bar{\alpha}({\rm H})\bar{\alpha}({\rm H_2O})C_6^{\rm Dis}({\rm H–H})C_6^{\rm Dis}({\rm H_2O–H_2O})}{\bar{\alpha}^2({\rm H})C_6^{\rm Dis}({\rm H_2O–H_2O}) + \bar{\alpha}^2({\rm H_2O})C_6^{\rm Dis}({\rm H–H})}, \quad (3)$$

where the electric dipole polarizabilities of the two monomers are $\bar{\alpha}({\rm H}) = 0.667$ Å^3 (Miller & Bederson 1978) and $\bar{\alpha}({\rm H_2O}) = 1.47$ Å^3, (Stone 2016), while $C_6^{\rm Dis}({\rm H_2O–H_2O}) = 45.4$ au (Smith et al. 2012) and $C_6^{\rm Dis}({\rm H–H}) = 6.499$ au (Mitroy & Bromley 2005).

One obtains $C_6^{\rm Dis}({\rm H–H_2O}) = 16.90$ au, which is about 90 per cent of $C_6^{\rm PES}$. The induction contribution is obtained from Ma, Zeng & Li (2014):

$$C_6^{\rm Ind} =< \mu_{\rm H_2O}^2 > \bar{\alpha}({\rm H}).$$

Using the experimental estimate ($\mu_{\rm H_2O} = 1.857D$: Shostak, Ebenstein & Muenter 1991) of the electric dipole moment of H_2O, one obtains $C_6^{\rm Ind} = 2.4$ au. The global experimental value of $C_6 = 19.3$ au is then in very good agreement with the PES value.

2.2 Dynamics

Both rigid asymmetric top (RAST-CC) and rigid-bender (RB-CC) close-coupling calculations were performed using our new PES and the NEWMAT code (Stoecklin et al. 2019). The RB-CC method includes the bending–rotation coupling explicitly for a bent (Stoecklin et al. 2019, 2021) or linear (Denis-Alpizar et al. 2013; Stoecklin et al. 2013; Al Mogren et al. 2014; Denis-Alpizar, Stoecklin & Halvick 2014, 2015; Stoecklin, Denis-Alpizar & Halvick 2015) triatomic molecule colliding with an atom.

The H_2O basis set included ten values of the water rotational quantum number j and two bending levels for the RB-CC calculations, leading to a maximum energy of 3994 cm^{-1} for the rovibrational basis set. Scattering calculations were performed separately for the ortho and para states of H_2O for collision energies up to 5000 cm^{-1}. The state-selected bending relaxation cross-sections are fitted using power laws in the [500, 5000] cm^{-1} interval and the resulting coefficients are used to compute bending relaxation rates above 500 K. Excited stretching modes of H_2O are not taken into account in the present work. The resulting error is expected to be very small, while taking place only for the highest energies.

The maximum propagation distance was $30a_0$, and convergence was checked as a function of propagator step size. Partial waves up to total angular momentum $J = 65$ were included in the calculations to achieve a 10^{-3} relative criterion for convergence of the state-selected quenching cross-section as a function of the maximal value of the total angular momentum quantum number J. This is in contrast with the He–H_2O system, for which $J = 125$ was needed to reach the same convergence criterion because of the differences in relative masses.

3 RESULTS

3.1 4D PES

The fitted and *ab initio* energies are in quite satisfactory agreement. The root-mean-square deviation in cm^{-1} (RMSD) is equal to 3.19×10^{-3} for negative energies and 2.94×10^{-2} for positive energies between 0 and 5000 cm^{-1}.

Downloaded from https://academic.oup.com/mnras/article/514/3/4426/6622022 by Universite de Bordeaux user on 01 July 2022

Table 1. Comparison between our results and those available in the literature for the equilibrium geometries and energies of the H–H_2O complex. (R is reported in Å, θ and φ in degrees, and energy in cm^{-1}).

PES	(R, θ, φ)	E_{min} (cm^{-1})
This work	(3.41, 122.53, 0)	−59.58
McCarver & Hinde (2021)	(3.41, 122.25, 0)	−61.3
Dagdigian & Alexander (2013)	(3.41, 119.04, 0)	−61.0
Zhang, Sabelli & Buch (1991)	(3.325, 127.74, 0)	−53 ± 6

The global minimum of the PES, −59.58 cm^{-1}, is obtained for the averaged (Valiron et al. 2008) bending angle $\gamma = 104.4°$ and is associated with a bent configuration (R = 3.41 Å, θ = 122.53°, φ = 0°) of the H_2O–H complex. These features are compared with those obtained by other teams in Table 1, where the present geometry of the complex appears to be very close to that obtained by Dagdigian & Alexander (2013) or in the very recent study of McCarver & Hinde (2021). The binding energy of the complex is also seen to be very close to the one obtained by these authors. It is, however, slightly smaller, as a result of our choice of using a slightly smaller basis set in order to be able to compute the large grid of points needed to describe the bending motion.

It is also interesting to compare these results with those obtained for the related He–H_2O complex (Stoecklin et al. 2021). The binding energy for H_2O–H is twice as large that of H_2O–He (−34.55 cm^{-1}), while the Jacobi angle of the complex is also larger than that of H_2O–He (θ = 76.43°).

Fig. 2 shows contour plots of the H–H_2O PES for different values of γ and φ. The H_2O–H PES is seen to exhibit a stronger dependence on the bending angle γ.

This point is illustrated further in Fig. 3, showing the comparison of several PES radial expansion coefficients $V_{lm}(R)$ for H_2O + H and H_2O + He (Stoecklin et al. 2021). The anisotropic terms show a clear dependence on the bending angle, which is much more pronounced in the case of H_2O + H. This fact, combined with the larger value

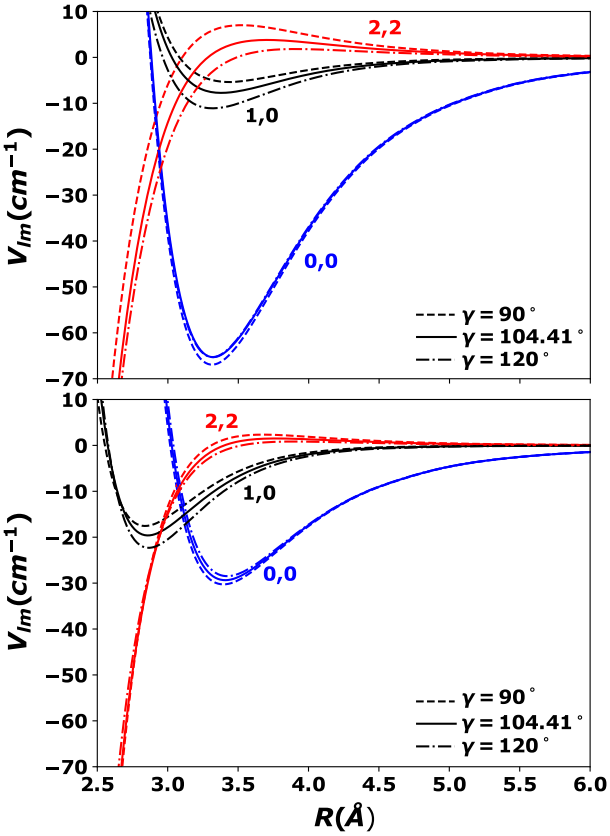

Figure 3. Variation of selected V_{lm} radial coefficients as a function of R for three different values of bending angle. The H_2O + H and H_2O + He PESs are shown in the top and bottom panels respectively. The l and m quantum numbers are reported for each group of curves.

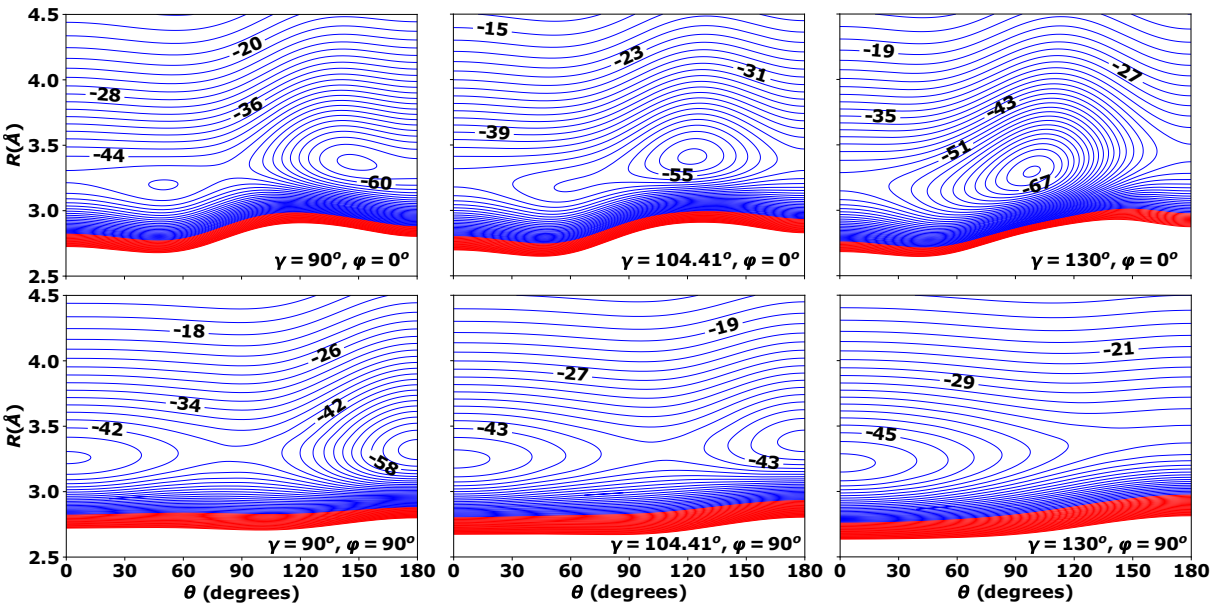

Figure 2. Contour plot of the H_2O + H complex for several values of the bending angle γ and azimuth φ. Negative and positive energies are reported in steps of 1 cm^{-1}.

Downloaded from https://academic.oup.com/mnras/article/514/3/4426/6622022 by Universite de Bordeaux user on 01 July 2022

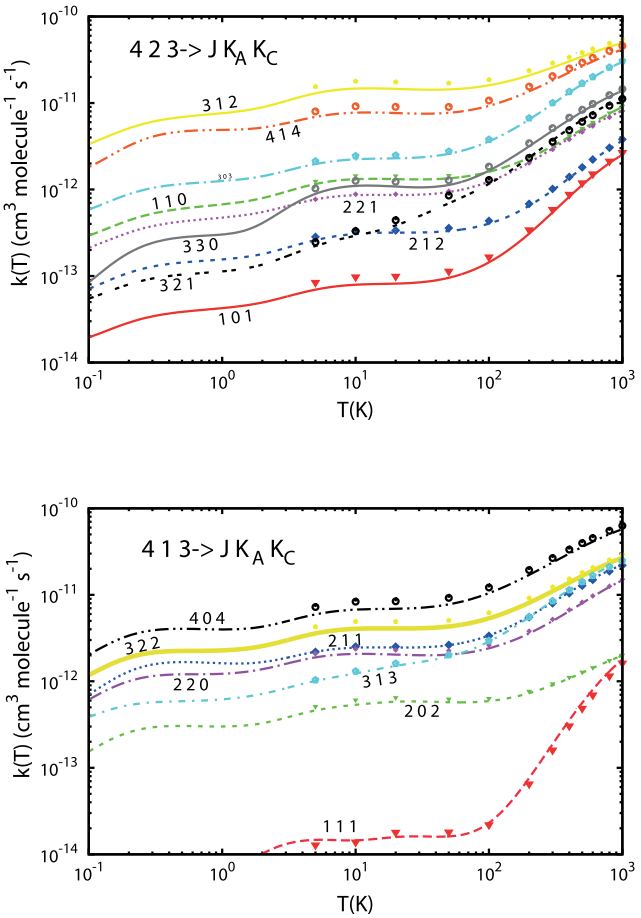

Figure 4. State-to-state rate coefficients induced by collision with H for the two initial states 4_{23} and 4_{13} of H_2O. The final rotational state is indicated on each curve. The continuous lines are our results, while the symbols are the values of Daniel et al. (2014) given in the Basecol database (Dubernet et al. 2013).

of the binding energy of the complex, is expected to favour coupling between bending and rotation and then to increase the efficiency of vibrational quenching.

3.2 Dynamics

3.2.1 Rotational transitions inside the fundamental bending level

Rigid-rotor calculations

RAST-CC calculations are performed inside the fundamental H_2O bending state and compared with those of the Basecol (Dubernet et al. 2013) data base. The Basecol data were calculated by Daniel et al. (2014) using the PES of Dagdigian & Alexander (2013). An example of a comparison between our results and those of Daniel et al. (2014) is shown in Fig. 4 for transitions issued from the 4_{03} or 4_{13} levels. The relative average difference between our results and those of Daniel et al. (2014) ranges from 5–40 per cent, as a result of the differences between the two PESs.

Rigid-rotor versus rigid-bender calculations

RB-CC calculations are compared with the present RAST-CC results in Fig. 5. The two kinds of calculation are in excellent agreement above 1 cm^{-1}, demonstrating that the rigid-rotor approximation safely describes rotational transitions inside the same bending level.

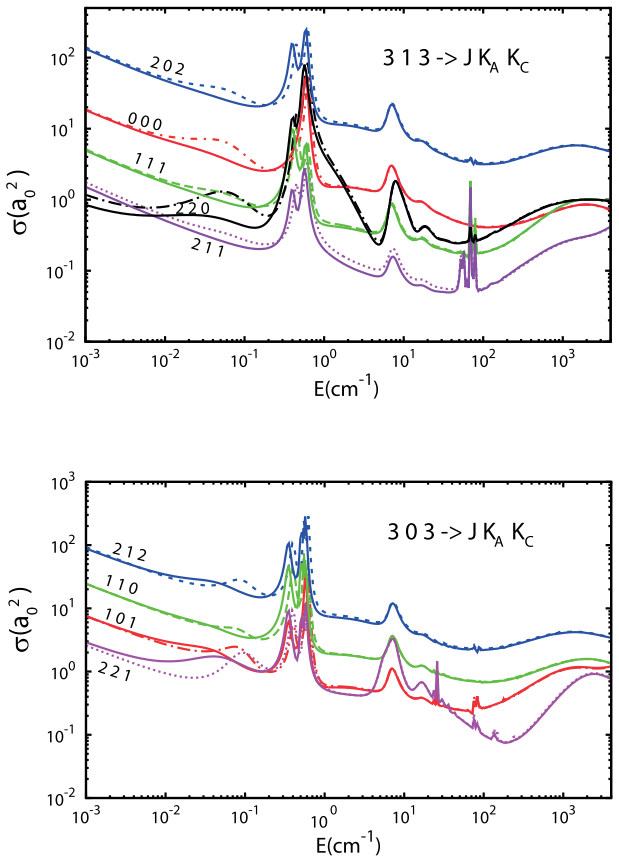

Figure 5. Comparison between the state-to-state RB-CC (dashed lines) and RAST-CC (continuous lines) rotational cross-sections starting from the ($\nu = 0$, 3_{03}) and ($\nu = 0$, 3_{13}) levels of H_2O colliding with H. The top and bottom panels are dedicated to *para* and *ortho* transitions, respectively.

3.2.2 Rotational transitions inside two different bending levels

General behaviour

State-to-state rotational cross-sections inside the bending levels $\nu_2 = 0$ and $\nu_2 = 1$ are shown in Fig. 6 for transitions from the 3_{03} and 3_{13} levels of H_2O. The curves associated with the same rotational transitions are very similar inside each of these two bending levels. The shapes of some of the resonances are only seen to differ slightly.

Fig. 6 also shows two examples of state-to-state cross-sections for rotational transitions inside $\nu_2 = 1$, differing from their counterparts inside $\nu_2 = 0$. These are the cases of the $3_{03} \rightarrow 2_{21}$ and $3_{13} \rightarrow 2_{20}$ transitions.

As discussed in our previous work (Stoecklin et al. 2021), this results from the coupling between bending and rotation, which makes the order of the states differ inside different bending levels. This is the case for the 2_{20} *para* state, which is below the 3_{13} level inside $\nu_2 = 0$, while the opposite applies inside $\nu_2 = 1$. A similar situation is found for the 2_{21} and 3_{03} *ortho* levels. Furthermore, highly excited rotational states in $\nu = 0$ may also be interspersed between rotational levels in $\nu = 1$ (e.g. $\nu_2 = 0$, 9_{64} with $\nu_2 = 1$, 0_{00} and $\nu_2 = 1$, 1_{11} in the *para* case, and $\nu_2 = 0$, 9_{63} with $\nu_2 = 1$, 1_{01} and $\nu_2 = 1$,1_{10} in the *ortho* levels). Therefore, some rotational cross-sections inside $\nu_2 = 0$ cannot be deduced from experimental measurements inside $\nu_2 = 1$ as is very often done.

Comparison with He–H_2O

In order to be able to perform comparisons with the He–H_2O system, in Fig. 6 we represented the same rotational transitions as

Downloaded from https://academic.oup.com/mnras/article/514/3/4426/6622022 by Universite de Bordeaux user on 01 July 2022

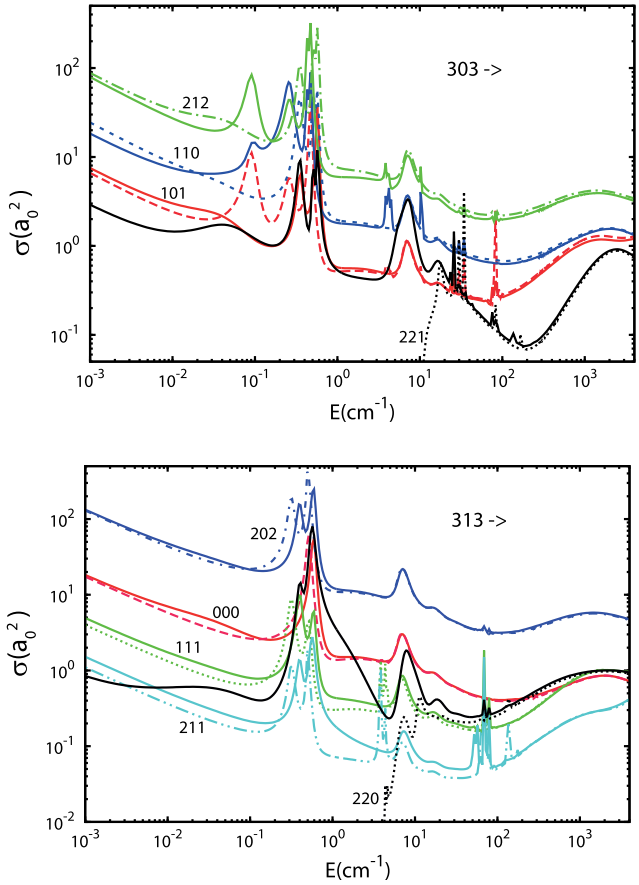

Figure 6. RB-CC rotational cross-sections starting from the 3_{03} and 3_{13} levels of H_2O colliding with H. Continuous and dashed lines are respectively associated with transitions inside $\nu_2 = 0$ and $\nu_2 = 1$. The *para* and *ortho* transitions are presented respectively in the higher an lower panels.

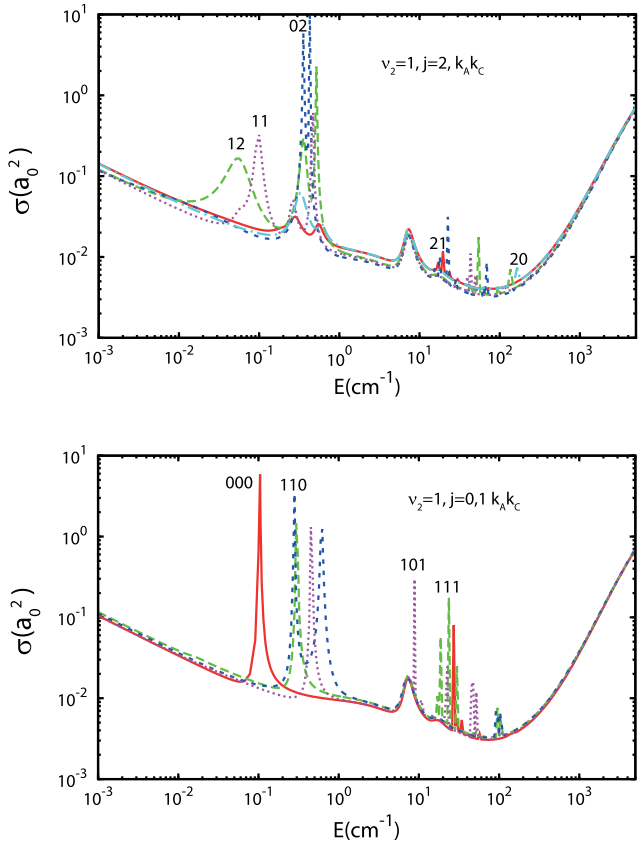

Figure 7. RB-CC cross-sections for the bending relaxation of H_2O ($\nu_2, j = 0, 1$) (lower panel) and H_2O ($\nu_2, j = 2$) (upper panel) induced by collision with H. The initial state rotational state is indicated by the values of $j\ K_A K_C$.

seen in fig. 5 of our previous work (Stoecklin et al. 2021). At first sight, the magnitudes of the cross-sections appear to be very similar for the two systems. A more careful comparison of the corresponding state-to-state rate coefficients was performed by (Daniel et al. 2014), who concluded that globally they are of the same order of magnitude. The well depth of H–H_2O is roughly double that of He–H_2O and one might expect rotational coupling to be more efficient for this system. This effect, however, is cancelled by the smaller relative mass of H–H_2O, which is only a fourth of that of He–H_2O.

3.2.3 Rotational transitions between two different bending levels

General behaviour

A first interesting feature of vibrational quenching is illustrated in Figs 7 and 8 where RB-CC cross-sections for each of the $j = 0, 1, 2$ and $j = 3, 4$ multiplets belonging to the first excited bending level $\nu_2 = 1$ of H_2O are presented.

For lower values of j, the vibrational quenching cross-section inside a multiplet does not vary much as a function of the initial rotational energy, while it increases monotonically for the highest values of j represented, suggesting that coupling between bending and rotation is efficiently at play. The *ortho* and *para* levels that are closest in energy are also seen to give almost the same vibrational cross-sections as noticed previously for the He–H_2O collision. This suggests that, if one is interested only in vibrational quenching-rate coefficients, it is sufficient for a given value of j to perform calculations for the symmetry leading to the largest number of states. In other words, for even or odd values of j one needs to perform calculations only for the para or ortho symmetry of H_2O, respectively.

The j-selected quenching-rate coefficients are represented in Fig. 9, where the global Boltzmann-averaged quenching-rate coefficient is also reported.

The ratio of the j-selected vibrational quenching-rate coefficients divided by that of the $j = 0$ state is also represented for $j = 1$, 2, 3, 4 in the upper panel of the same figure as a function of temperature. This figure clearly shows three regimes. At very low temperature, the long range of the PES is controlling the collision and is not strong enough to favour the coupling between bending and rotation. As a result, vibrational quenching is most efficient for $j = 2$ and decreases for higher values of j. At higher intermediate temperature, the well is at play and the efficiency of bending relaxation increases monotonically with the rotational excitation as a result of the coupling between bending and rotation. The coupling efficiency reaches a maximum at about 150, 200, and 220 K, respectively, for $j = 2$, 3, and 4, before decreasing when the temperature keeps increasing. These maxima were obtained for lower temperatures in the case of He–H_2O, as a result of the smaller value of the well depth for this system. For higher temperatures, the mechanism is more complicated, as it involves the repulsive part of the PES.

Comparison with He–H_2O

From the comparison of Fig. 9 with the corresponding Fig. 7 for the He–H_2O system (Stoecklin et al. 2021), we see that vibrational quenching of H_2O is about three orders of magnitude larger for

Downloaded from https://academic.oup.com/mnras/article/514/3/4426/6622022 by Universite de Bordeaux user on 01 July 2022

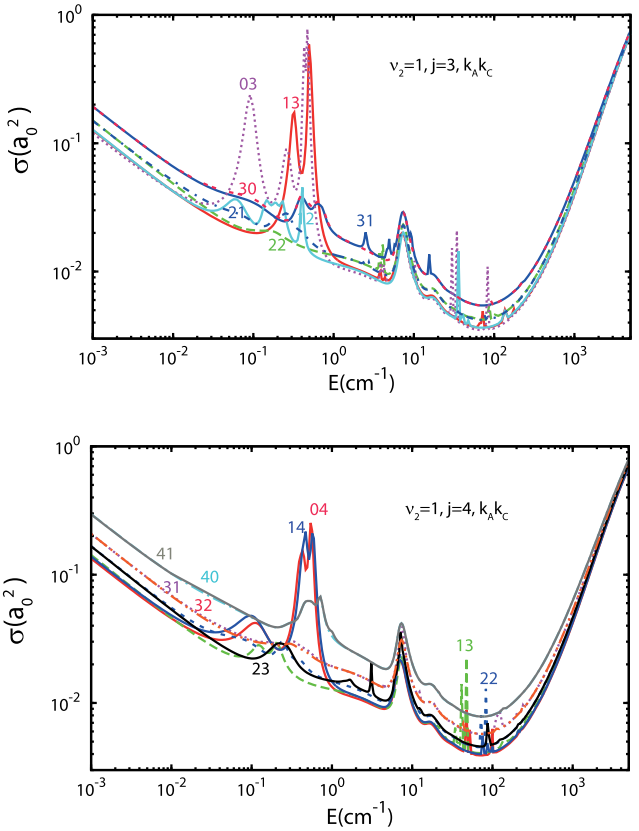

Figure 8. RB-CC cross-sections for the bending relaxation of H_2O ($\nu_2, j = 4$) (lower panel) and H_2O ($\nu_2, j = 3$) (upper panel) induced by collision with H. The initial state rotational state is indicated by the values of $K_A K_C$.

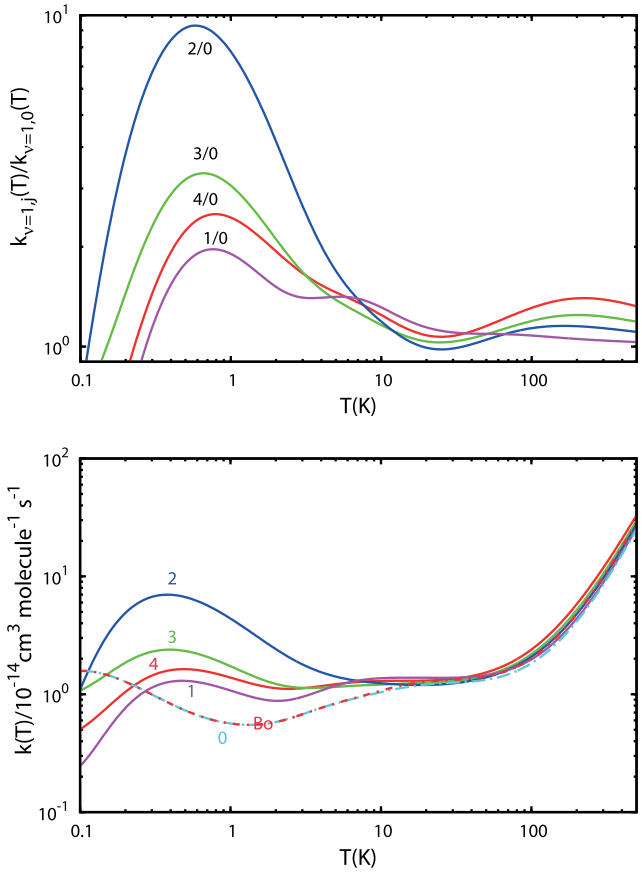

Figure 9. Comparison of the Boltzmann-averaged (denoted Bo) and state-selected RB-CC vibrational quenching-rate coefficients of H_2O ($\nu_2 = 1$, $j = 0, 1, 2, 3, 4$) induced by collision with H. The initial rotational state is indicated by the values of j. The higher panel shows the ratio of the j-selected vibrational quenching-rate coefficients divided by that of the $j = 0$ state as a function of temperature for $j = 1, 2, 3, 4$.

collisions with H than for He, for the whole range of temperatures. Vibrational quenching of H_2O is then more efficient with H than with He, in contrast with rotational quenching, which is of the same order of magnitude for the two systems. This may be attributed to the more attractive potential of the H–H_2O system, the well depth of which is double that of He–H_2O. Such an effect which was found to be important for the vibrational quenching of ionic molecules. The issues discussed by Stoecklin et al. (2016) also seem to be at play here, as discussed in Section 3.1.

4 SUMMARY

A quantum study of the bending relaxation of H_2O by collision with H was presented. With this aim, a new 4D PES including the bending of H_2O was first developed. The collisional dynamics was then investigated by comparing rigid-rotor and rigid-bender close-coupling calculations, which include the bending degree of freedom. As expected, they are found to be in excellent agreement above 1 cm^{-1} for rotational transitions inside the same bending level. Rotational transitions inside the same bending level are therefore safely described by using the rigid-rotor approximation, provided a rigid-rotor PES calculated for this peculiar bending level is used. Our results were also compared with equivalent rigid-rotor data available in the Basecol database. The relative difference between our results and those of Daniel et al. (2014) ranges between 5 and 40 per cent, as a result of both differences between the two PESs and the rotational basis set used for the dynamics by Daniel et al. (2014).

We find, in agreement with these authors, that the magnitudes of the state-to-state rotationally inelastic rate coefficients are globally of the same order as those of He–H_2O. This is in contrast with the bending relaxation of H_2O, which is found to be about three orders of magnitude larger for collisions with H than for those with He for the whole range of temperatures considered in the present work. This result is attributed to the deeper well of the H–H_2O PES, which is expected to favour coupling between bending and rotation. We confirm the result noted in our previous work dedicated to He–H_2O that the *ortho* and *para* levels closest in energy give almost the same vibrational cross-sections. This suggests that, at least for these two systems, it is sufficient, for each value of j, to perform calculations for the symmetry leading to the largest number of states. In other words, for even or odd values of j, one needs to perform calculations only for the *para* or *ortho* symmetry of H_2O, respectively.

Above 30 K, the efficiency of H_2O collisional bending relaxation is also found to increase with rotational excitation as a result of the coupling between bending and rotation, and to reach a maximum between 100 and 200 K, depending on the initial value of j. Conversely, the coupling efficiency appears to be less efficient at low and high temperatures, as the dynamics in these regions is not controlled by the well.

Downloaded from https://academic.oup.com/mnras/article/514/3/4426/6622022 by Universite de Bordeaux user on 01 July 2022

ACKNOWLEDGEMENTS

This work was supported by the French Agence Nationale de la Recherche (ANR-Waterstars), Contract No. ANR-20-CE31-0011. We acknowledge support from ECOS-SUD-CONICYT project number C17E06 (Programa de Cooperación Científica ECOS-CONICYT ECOS170039). LDCH is also thankful for support from ANID BECAS/DOCTORADO NACIONAL 21210379. Computer time for this study was provided by the Mésocentre de Calcul Intensif Aquitain, which is the computing facility of Université de Bordeaux et Université de Pau et des Pays de l'Adour.

DATA AVAILABILITY

The data underlying this study are available in this work, and the computed rate coefficients will also be made available in the Basecol and Lamda databases.

REFERENCES

Al Mogren M. M., Denis-Alpizar O., Abdallah D. B., Stoecklin T., Halvick P., Senent M.-L., Hochlaf M., 2014, J. Chem. Phys., 141, 044308
Ayouz M., Faure A., Tennyson J., Tudorovskaya M., Kokoouline V., 2021, Atoms, 9, 62
Baudry A. et al., 2018, A&A, 609, A25
Boys S. F., Bernardi F., 1970, Mol. Phys., 19, 553
Dagdigian P. J., Alexander M. H., 2013, J. Chem. Phys., 139, 194309
Daniel F., Faure A., Dagdigian P. J., Dubernet M.-L., Lique F., Forêts G. P. D., 2014, MNRAS, 446, 2312
Denis-Alpizar O., Stoecklin T., Halvick P., Dubernet M.-L., 2013, J. Chem. Phys., 139, 034304
Denis-Alpizar O., Stoecklin T., Halvick P., 2014, J. Chem. Phys., 140, 084316
Denis-Alpizar O., Stoecklin T., Halvick P., 2015, MNRAS, 453, 1317
Dubernet M. et al., 2013, A&A, 553, 50
Dunning T. H., 1989, J. Chem. Phys., 90, 1007
Fu B., Zhang D. H., 2013, J. Chem. Phys., 138, 184308
Gray M., Baudry A., Richards A., Humphreys E., Sobolev A., Yates J., 2016, MNRAS, 456, 374
Hirota T., Kim M. K., Honma M., 2016, ApJ, 817, 168
Ho T. S., Rabitz H., 1996, J. Phys. Chem., 104, 2584
Hou D., Ma Y.-T., Zhang X.-L., Li H., 2016, J. Chem. Phys., 144, 014301
Hunter T., Young K., Christensen R., Gurwell M., 2007, Proc. IAU, 3, 481
Jiang B., Xie D., Guo H., 2011, J. Chem. Phys., 135, 084112
Ma Y.-T., Zeng T., Li H., 2014, J. Chem. Phys., 140, 214309
McCarver G. A., Hinde R. J., 2021, J. Chem. Phys., 155, 114302
Menten K. M., Melnick G. J., 1989, ApJ, 341, L91
Menten K. M., Young K., 1995, ApJ, 450, L67
Miller T. M., Bederson B., 1978, Adv. At. Mol. Phys., 13, 1
Mitroy J., Bromley M. W. J., 2005, Phys. Rev. A, 71, 032709
Nesterenok A., 2015, MNRAS, 449, 2875
Shostak S. L., Ebenstein W. L., Muenter J. S., 1991, J. Chem. Phys., 94, 5875
Smith Q. A., Ruedenberg K., Gordon M. S., Slipchenko L. V., 2012, J. Chem. Phys., 136, 244107
Stoecklin T., Denis-Alpizar O., Halvick P., Dubernet M.-L., 2013, J. Chem. Phys., 139, 124317
Stoecklin T., Denis-Alpizar O., Halvick P., 2015, MNRAS, 449, 3420
Stoecklin T., Halvick P., Gannouni M. A., Hochlaf M., Kotochigova S., Hudson E. R., 2016, Nature Commun., 7, 11234
Stoecklin T., Denis-Alpizar O., Clergerie A., Halvick P., Faure A., Scribano Y., 2019, J. Phys. Chem. A, 123, 5704
Stoecklin T., Cabrera-González L. D., Denis-Alpizar O., Páez-Hernández D., 2021, J. Chem. Phys., 154, 144307
Stone A., 2016, The Theory of Intermolecular Forces. Oxford University Press, Oxford, UK. https://books.google.cl/books?id = jPjsjwEACAAJ
Valiron P., Wernli M., Faure A., Wiesenfeld L., Rist C., Kedžuch S., Noga J., 2008, J. Chem. Phys., 129, 134306
Van Dishoeck E. F., Herbst E., Neufeld D. A., 2013, Chem. Rev., 113, 9043
Werner H.-J., Knowles P. J., Knizia G., Manby F. R., Schütz M., 2012, WIREs Comput. Mol. Sci., 2, 242
Zhang Q., Sabelli N., Buch V., 1991, J. Chem. Phys., 95, 1080

This paper has been typeset from a TEX/LATEX file prepared by the author.

Downloaded from https://academic.oup.com/mnras/article/514/3/4426/6622022 by Universite de Bordeaux user on 01 July 2022